AIAA JOURNAL
Vol. 39, No. 2, February 2001

Synchronous Hopf-Bifurcation and Damping Osmosis Phenomena of Liquid–Spacecraft Coupled System

Xingyu Gou*
Beijing Institute of Control Engineering, Beijing 100080, People's Republic of China
Xingrui Ma†
China Space Science and Technology Corporation, Beijing 100830, People's Republic of China
Benli Wang‡
Harbin Institute of Technology, Harbin 150001, People's Republic of China
Tieshou Li§
Beijing Institute of Control Engineering, Beijing 100080, People's Republic of China
and
Huaide Huang¶
Chinese Academy of Launch-Vehicle Technology, Beijing 100076, People's Republic of China

Nonlinear dynamics of a liquid–spacecraft coupled system are investigated. The spacecraft is modeled on a spring–damper–mass system, and the liquid is inside a rigid cylindrical tank attached to the mass with and without an annular baffle. A group of nonlinear dynamic differential equations is derived by Lagrange's method and symbolic operations using the software *Mathematica*. The symmetry of the equations verifies their correctness. Numerical simulations and amplitude-frequency response analyses show that the so-called synchronous Hopf bifurcation takes place in the nonplanar sloshing modes of the system without a baffle. Also, the baffle and the damper have different effects on the damping behavior of the vibration and the sloshing, so that the concept of damping osmosis in nonlinear coupled systems is described.

Nomenclature

A_i	=	standard orthogonal coefficient of ψ_i
a_x, a_y	=	acceleration in X and Y directions, respectively
B_n	=	standard orthogonal coefficient of ξ_n
c_x, c_y	=	damping constant in X and Y directions in the coupled system
D	=	mean depth of an annular baffle immerged in the liquid, cm
d	=	tank diameter, cm
E_{ex}, E_{ey}	=	nondimensional amplitude of the excitation force
F_{ex}, F_{ey}	=	amplitude of the excitation force
$\{F\}_{6\times 1}$	=	right side functions vector of Eq. (22)
$f(r)$	=	static free surface equilibrium shape function
g	=	uniform gravity or acceleration, $\mathrm{m}\cdot\mathrm{s}^{-2}$
h	=	average depth of the liquid in the tank, cm
$\boldsymbol{i}, \boldsymbol{j}, \boldsymbol{k}$	=	unit vectors along the coordinate axes $oxyz$ attached to the cylindrical tank
k	=	spring rigidity in X and Y directions
k_n, k_{ij}	=	radial wave numbers of ψ_n
L	=	Lagrangian of the coupled system
ℓ_{rn}	=	element of the nonlinear wavelength transformation matrix from $\{\dot{q}_n\}$ to $\{\phi_n\}$
$\ell_{nn}^{(0)}$, $\ell_{mni}^{(1)}$, $\ell_{mnij}^{(2)}$	=	coefficients of ℓ_{mn} induced by series of complicated modal integrals
M	=	overall mass of the cylindrical tank and the dry mass
$[\tilde{M}]_{6\times 6}$	=	nondimensional time-varying mass matrix of the nonlinear coupled system
$OXYZ$	=	initial coordinate
$oxyz$	=	coordinate attached to the tank
$or\theta z$	=	corresponding cylindrical coordinate of $oxyz$
p_g	=	gas pressure above the liquid surface
p_L	=	liquid pressure
q_i	=	generalized coordinates of η
$\boldsymbol{R}$	=	absolute velocity of the liquid mass point
S	=	cross section of the cylindrical tank
T_l	=	kinetic energy of the liquid
T_M	=	kinetic energy of the dry mass M
U_G	=	gravity position potential energy of the liquid
U_k	=	potential energy of the springs
U_σ	=	surface tension potential energy of the liquid
V	=	volume of the liquid in the tank
w	=	width of the annular baffle, cm
Γ	=	linear hysteresis constant of the contact angle of liquid on the solid wall of the tank
δ	=	logarithm decay damping of the free sloshing
ε	=	orders of maglitude of the primary modes sloshing
ζ_x, ζ_i	=	damping ratio
ζ_{xs}, ζ_{xl}	=	small and large damping ratio of the elastic vibration
η	=	wave height of the free surface measured from the mean equilibrium height
$\eta_{\max}$	=	maximum of the sloshing height
λ_{ij}	=	radial wave numbers of ξ_n with the linear hysteresis of the contact angle being considered[4]
μ	=	nondimensional mass ratio
ν_a, ν_b	=	two linear coupled frequencies of the coupled system
ν_n	=	nondimensional frequency ratio of each order sloshing frequency to the characteristic frequency of the spring–mass system
ν_x	=	nondimensional frequency of excitation
ξ_n	=	modal shapes of $\eta(r, \theta, t)$
ρ	=	density of the liquid

Received 31 July 1999; revision received 20 March 2000; accepted for publication 13 July 2000. Copyright © 2000 by the authors. Published by the American Institute of Aeronautics and Astronautics, Inc., with permission.

*Senior Engineer, Spacecraft Control Concept and Dynamics Simulation Laboratory, P.O. Box 2729.
†Vice-President and Doctoral Tutor, P.O. Box 849-A1.
‡Professor and Doctoral Tutor, Department of Space Engineering and Mechanics.
§Professor and Doctoral Tutor, Spacecraft Control Concept and Dynamics Simulation Laboratory, P.O. Box 2729.
¶Professor, Committee of Science and Technology; currently retired.

σ = surface tension coefficient of the liquid
ϕ = liquid flow potential function
ϕ_i = generalized coordinates of $\phi(r, \theta, z, t)$
ψ_i = modal shapes of $\phi(r, \theta, z, t)$
$2H$ = mean curvature of the free surface

Introduction

In the space engineering field, dynamic coupling related to liquid sloshing is encountered frequently.[1] A linear equivalent mechanical model, that is, either a spring–mass or a simple pendulum, is used to describe sloshing and to predict the motion of the coupled liquid–spacecraft system.[2,3] However, the liquid sloshing is an intrinsic nonlinear problem. In particular, finite-amplitude sloshing must be described by a nonlinear model. During the launch phase, docking and separation or maneuvering, large-amplitude liquid sloshing would take place. The sloshing in a low gravity environment may be nonlinear when the carrier spacecraft rotates slowly. Therefore, finite-amplitude sloshing has been important for a long time.

The nonlinear analytical study of sloshing is not easy, and the nonlinearly coupled dynamics of a liquid–spacecraft system with a general mode is even more difficult. Peterson et al.[4] adopted an oscillator to represent the linear vibration of spacecraft. In their model, a cylindrical tank is fixed on the mass of the oscillator. By unique experiments and a theoretical model, they investigated the nonlinearly coupled dynamic behavior of the model. This is a simple and efficient model to study the nonlinear-coupled mechanism. New liquid–spacecraft coupled modes are formed, and nonlinear multifrequency resonance becomes more complicated due to the participation of the coupled modes.

The finite-amplitude sloshing in the coupled model has some unique characteristics that distinguish it from the sloshing in uncoupled cases. It should not be assumed that a linear model or even a nonlinear uncoupled model will lead to an accurate analytical model if sloshing and spacecraft motion are closely coupled. Van Schoor and Crawley[5] studied this model by use of both ground and flight tests. These tests show that the influence of the bottom shape of the tank is negligible, but that the gravity magnitude and the type of liquid will affect the dynamic behavior considerably.

In this paper, a group of coupled dynamic differential equations is established based on the model of Peterson et al.[4] by symbolic operation of the software *Mathematica*. The damping of the annular baffle is introduced. Numerical simulations show that the mathematical model of the coupled system can predict the bifurcation of the nonplanar sloshing modes seen in the experiment of Ref. 4 without a baffle and that the baffle suppresses the sloshing significantly but has different effects on the elastic vibration depending on the excitation frequency.

Dynamic Model

The system studied is represented schematically in Fig. 1. The tank is suspended by springs and dampers. The uniform gravity field gk is aligned with the cylinder axis and is sufficient to collect the liquid at the bottom of the tank.

For a small Bond number, the static free surface of the liquid is like a meniscus. The origin of the coordinate system $oxyz$ is at the center of the mean static surface.

Finite-Amplitude Sloshing

The liquid is assumed to be inviscid, irrotational, and incompressible, and the finite-amplitude sloshing of the liquid can be described according to the potential theory as follows:

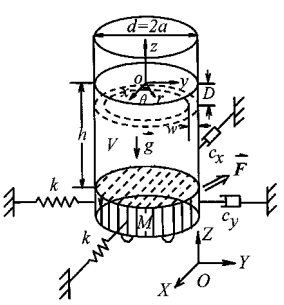

Fig. 1 Dynamic model of a lateral liquid-spacecraft coupled system.

$$\nabla^2\phi = 0 \qquad \text{in} \qquad V \tag{1}$$

$$\frac{\partial\phi}{\partial r} = 0 \qquad \text{on} \qquad r = a \tag{2}$$

$$\frac{\partial\phi}{\partial z} = 0 \qquad \text{on} \qquad z = -h \tag{3}$$

$$\frac{\partial\eta}{\partial t} + \nabla\phi\cdot\nabla\eta = \frac{\partial\phi}{\partial z} \qquad \text{on} \qquad z = \eta \tag{4}$$

$$\frac{2\sigma H}{\rho} - \frac{\partial\phi}{\partial t} - \frac{1}{2}|\nabla\phi|^2 - g\eta - (a_x x + a_y y) = \frac{p_g - p_L}{\rho} \qquad \text{on} \qquad z = \eta \tag{5}$$

where Eqs. (2) and (3) are the boundary conditions on the solid wall and Eqs. (4) and (5) are the kinematic and dynamic boundary conditions on the free surface, respectively.

For the linear sloshing problem, the terms of second and higher orders in Eq. (4) and (5) are neglected, and it is evident that the potential function is of the same order as the wave height and that the eigenfunctions can be obtained from Eqs. (1–4).

For the nonlinear sloshing problem, there are many means to deal with the preceding equations. The method of functional extremum by Miles[6] was generalized by Peterson et al.[4] to obtain the nonlinear wavelength transformation between the generalized coordinates of the velocity potential and the wave height function.

The method of Peterson et al.[4] uses the modal coordinates, modal velocities, and modal accelerations to describe finite-amplitude nonlinear sloshing and, therefore, is intuitive and distinct. Hutton[7] combined the kinematics with the dynamic condition to eliminate the wave height and then expanded the velocity potential according to the eigenfunctions to establish the dynamic differential equations of the generalized coordinates. With regard to the rectangular tanks, Nagata[8] perturbed the potential function to obtain the results after the elimination of the wave height. In 1987, Komatsu[9] put forward a method that retains both kinds of generalized coordinates and is applicable for tanks with arbitrary geometry. We obtain the wavelength transformation relationship directly from the kinematic boundary condition Eq. (4).

For a small Bond number, the following modal expansion is introduced:

$$\phi(r, \theta, r, t) = \sum_{i=1}^{N} \frac{\cosh k_i(z+h)}{\cosh k_i h}\psi_i(r, \theta)\phi_i(t) \tag{6}$$

$$\eta(r, \theta, t) = f(r) + \sum_{n=1}^{N} \xi_n(r, \theta)q_n(t) \tag{7}$$

According to Peterson et al.[4] and Miles,[10] five liquid modes are sufficient to obtain good accuracy; they are shown in Table 1.

Because the vibration of mass M couples to the primary modes, the vibrations along X and Y are both of the order of ε. All other modes are of the order of ε^2, and among them, ψ_3, ψ_4, and ψ_5 (ξ_3, ξ_4, and ξ_5) are dominant. Substituting expansions (6) and (7) into Eq. (4), we obtain

$$\sum_{n=1}^{N} P_n\phi_n = \sum_{n=1}^{N} \xi_n\dot{q}_n \tag{8}$$

where

$$P_n = Q_n + \sum_{i=1}^{N} Q_{ni}q_i, \qquad Q_n = k_n\psi_n\tanh k_n h - f'(r)\frac{\partial\psi_n}{\partial r}$$

$$Q_{ni} = -\nabla\psi_n\cdot\nabla\xi_i \tag{9}$$

Multiplying the two sides of Eq. (8) by ξ_m, $m = 1, 2, \ldots, N$, and integrating the results over the cross section S, we obtain

$$[I_{mn}]_{N\times N}\{\phi_n\}_{N\times 1} = \{\dot{q}_n\}_{N\times 1} \tag{10}$$

which can be rewritten as

$$\{\phi_n\}_{N\times 1} = [\ell_{mn}]_{N\times N}\{\dot{q}_n\}_{N\times 1} \tag{11}$$

Table 1 Assumed modes for nonlinear sloshing in cylindrical tanks

Modal index	Name	Order	ψ_n	ξ_n	Nodal diameter
1	Planar primary	ε	$A_1 J_1(k_{11}r)\cos\theta$	$B_1 J_1(\lambda_{11}r)\cos\theta$	1
2	Nonplanar primary	ε	$A_2 J_1(k_{11}r)\sin\theta$	$B_2 J_1(\lambda_{11}r)\sin\theta$	1
3	Axisymmetric secondary	ε^2	$A_3 J_0(k_{01}r)$	$B_3 J_0(\lambda_{01}r)$	0
4	Planar secondary	ε^2	$A_4 J_2(k_{21}r)\cos 2\theta$	$B_4 J_2(\lambda_{21}r)\cos 2\theta$	2
5	Nonplanar secondary	ε^2	$A_5 J_2(k_{21}r)\sin 2\theta$	$B_5 J_2(\lambda_{21}r)\sin 2\theta$	2

where

$$[\ell_{mn}]_{N\times N} = [I_{mn}]^{-1}_{N\times N}, \qquad I_{mn} = J_{mn} + \sum_{i=1}^{N} J_{mni} q_i$$

$$J_{mn} = \frac{1}{S}\iint_S \xi_m Q_n \,\mathrm{d}S, \qquad J_{mni} = \frac{1}{S}\iint_S \xi_m Q_{ni}\,\mathrm{d}S \tag{12}$$

It is evident that, even for $N = 5$, the inverse operation will be very cumbersome, and so we use *Mathematica* to obtain the inverse matrix:

$$\ell_{mn} \doteq \delta_{mn}\ell^{(0)}_{nn} + \sum_{i=1}^{N}\ell^{(1)}_{mni} q_i + \sum_{i=1}^{N}\sum_{j=1}^{N}\ell^{(2)}_{mnij} q_i q_j + \cdots \tag{13}$$

According to the physical meaning of the mathematical modal, finite-amplitude sloshing in the deep cylindrical tank must exhibit weak nonlinear dynamic behavior evolving from small-amplitude sloshing. Thus, the high-order terms included in the ellipsis can be neglected.

Based on the wavelength transformation relationship (13), the kinetic energy and potential energy of the liquid in the tank can be derived with q_i and $\dot{q}_i$, $i = 1, 2, \ldots, N$, as the generalized coordinates and velocities. The kinetic energy is given by

$$T_l = \frac{1}{2}\rho\iiint_V \dot{\boldsymbol{R}}\cdot\dot{\boldsymbol{R}}\,\mathrm{d}V \tag{14}$$

where

$$\dot{\boldsymbol{R}} = \dot{X}\boldsymbol{i} + \dot{Y}\boldsymbol{j} + \nabla\phi \tag{15}$$

The potential energy of the liquid is composed of the energy due to gravity by specifying the potential of the static equilibrium to be zero:

$$U_G = \iiint_V \rho g z\,\mathrm{d}V = \rho g\iint_S\left(\int_{f(r)}^{\eta(r,\theta,t)} z\,\mathrm{d}z\right)\mathrm{d}S \tag{16}$$

and the surface-tension potential

$$U_\sigma = \sigma\iint_S\sqrt{1+\nabla\eta\cdot\nabla\eta}\,\mathrm{d}S - \sigma\iint_S\sqrt{1+f'(r)\cdot f'(r)}\,\mathrm{d}S \tag{17}$$

Damping of the Annular Baffle

Modeling the damping is an important and difficult step in theoretical analysis and engineering in the process of deriving the dynamic equations. It usually depends on experiments. In engineering, an annular baffle is usually used to suppress the liquid sloshing. Miles[11] introduced a semi-empirical formula for the logarithmic decay damping for the annular baffle

$$\delta = 6\sqrt{2}\pi\left[1-\left(1-\frac{w}{a}\right)^2\right]^{\frac{3}{2}}\exp\left(-4.6\frac{D}{a}\right)\sqrt{\frac{\eta_{\max}}{d}} \tag{18}$$

This formula was obtained only for planar sloshing. Based on the geometrical symmetry of the tank, the empirical equation should be generalized to the finite-amplitude sloshing, which comprises both the nonplanar and symmetrical modes.

In Table 1, for the normalized modal shapes $B_1 = B_2$ and $B_4 = B_5$, the wave height can be rewritten as

$$\eta = f(r) + B_1 J_1(\lambda_{11}r)\sqrt{q_1^2+q_2^2}\sin\left[\theta + \tan^{-1}(q_1/q_2)\right] + B_3 J_0(\lambda_{01}r)q_3 + B_4 J_2(\lambda_{21}r)\sqrt{q_4^2+q_5^2} \times \sin\left[\theta + \tan^{-1}(q_4/q_5)\right] \tag{19}$$

Considering that the order of magnitude of q_3, q_4, and q_5 is lower than that of q_1 and q_2 and the characteristics of the Bessel modal parts $J_1(\lambda_{11}r)$, $J_0(\lambda_{01}r)$, and $J_2(\lambda_{21}r)$, we have approximately

$$\eta_{\max} = B_1 J_1(\lambda_{11}a)\sqrt{q_1^2+q_2^2} - B_3 J_0(\lambda_{01}a)|q_3| + B_4 J_2(\lambda_{21}a)\sqrt{q_4^2+q_5^2} \tag{20}$$

Dynamic Equations and Their Symmetry

The Lagrangian of the coupled system is

$$L = T_M + T_l - U_k - U_G - U_\sigma \tag{21}$$

Expanding expression (21) in terms of $X, Y, q_1, q_2, \ldots, q_5$ leads to several nonlinear equations of motion. Following Ref. 4, we write all parameters and variables in dimensionless form with respect to M, d, and/or $\sqrt{(k/M)}$ and obtain

$$(1+\mu)\ddot{X} + 2\zeta_x\dot{X} + X + \alpha_1\ddot{q}_1 = E_{ex}\cos\nu_x t \tag{22a}$$

$$(1+\mu)\ddot{Y} + 2\zeta_y\dot{Y} + Y + \alpha_2\ddot{q}_2 = E_{ey}\cos\nu_y t \tag{22b}$$

$$\begin{aligned}
&\mu_{11}\left(\ddot{q}_1 + 2\zeta\nu_1\dot{q}_1 + \nu_1^2 q_1\right) + \alpha_1\ddot{X} + \left(\beta_{111}q_1 + \beta_{112}q_2 + \beta_{113}q_3 + \beta_{114}q_4 + \beta_{115}q_5 + \beta_{1111}q_1^2 + \beta_{1112}q_1q_2 + \beta_{1122}q_2^2\right)\ddot{q}_1 \\
&+ \tfrac{1}{2}\left(\beta_{121}q_1 + \beta_{122}q_2 + \beta_{123}q_3 + \beta_{124}q_4 + \beta_{125}q_5 + \beta_{1211}q_1^2 + \beta_{1212}q_1q_2 + \beta_{1222}q_2^2\right)\ddot{q}_2 + \tfrac{1}{2}(\beta_{131}q_1 + \beta_{132}q_2)\ddot{q}_3 \\
&+ \tfrac{1}{2}(\beta_{141}q_1 + \beta_{142}q_2)\ddot{q}_4 + \tfrac{1}{2}(\beta_{151}q_1 + \beta_{152}q_2)\ddot{q}_5 + \left(\tfrac{1}{2}\beta_{111} + \beta_{1111}q_1 + \tfrac{1}{2}\beta_{1112}q_2\right)\dot{q}_1^2 + \left[\tfrac{1}{2}(\beta_{122} - \beta_{221}) + \left(\tfrac{1}{2}\beta_{1212} - \beta_{2211}\right)q_1 + \left(\beta_{1222} - \tfrac{1}{2}\beta_{2212}\right)q_2\right]\dot{q}_2^2 \\
&+ (\beta_{112} + \beta_{1112}q_1 + 2\beta_{1122}q_2)\dot{q}_1\dot{q}_2 + \beta_{113}\dot{q}_1\dot{q}_3 + \beta_{114}\dot{q}_1\dot{q}_4 + \beta_{115}\dot{q}_1\dot{q}_5 + \tfrac{1}{2}(\beta_{123} + \beta_{132} - \beta_{231})\dot{q}_2\dot{q}_3 + \tfrac{1}{2}(\beta_{124} + \beta_{142} - \beta_{241})\dot{q}_2\dot{q}_4 + \tfrac{1}{2}(\beta_{125} + \beta_{152} - \beta_{251})\dot{q}_2\dot{q}_5 + \sigma_{113}q_1q_3 \\
&+ \sigma_{114}q_1q_4 + \sigma_{125}q_2q_5 + \sigma_{1111}q_1^3 + \sigma_{1122}q_1q_2^2 = 0
\end{aligned} \tag{22c}$$

$$\mu_{22}\left(\ddot{q}_2 + 2\zeta\nu_2\dot{q}_2 + \nu_2^2 q_2\right) + \alpha_2\ddot{Y} + \tfrac{1}{2}\left(\beta_{121}q_1 + \beta_{122}q_2 + \beta_{123}q_3 + \beta_{124}q_4 + \beta_{125}q_5 + \beta_{1211}q_1^2 + \beta_{1212}q_1q_2 + \beta_{1222}q_2^2\right)\ddot{q}_1 + \left(\beta_{221}q_1 + \beta_{222}q_2 + \beta_{223}q_3 + \beta_{224}q_4 + \beta_{225}q_5 + \beta_{2211}q_1^2 + \beta_{2212}q_1q_2 + \beta_{2222}q_2^2\right)\ddot{q}_2 + \tfrac{1}{2}(\beta_{231}q_1 + \beta_{232}q_2)\ddot{q}_3 + \tfrac{1}{2}(\beta_{241}q_1 + \beta_{242}q_2)\ddot{q}_4 + \tfrac{1}{2}(\beta_{251}q_1 + \beta_{252}q_2)\ddot{q}_5 + \left[\tfrac{1}{2}(\beta_{121} - \beta_{112}) + \left(\beta_{1211} - \tfrac{1}{2}\beta_{1112}\right)q_1 + \left(\tfrac{1}{2}\beta_{1212} - \beta_{1122}\right)q_2\right]\dot{q}_1^2 + \left[\tfrac{1}{2}\beta_{222} + \tfrac{1}{2}\beta_{2212}q_1 + \beta_{2222}q_2\right]\dot{q}_2^2 + (\beta_{221} + 2\beta_{2211}q_1 + \beta_{2212}q_2)\dot{q}_1\dot{q}_2 + \tfrac{1}{2}(\beta_{123} + \beta_{231} - \beta_{132})\dot{q}_1\dot{q}_3 + \tfrac{1}{2}(\beta_{124} + \beta_{241} - \beta_{142})\dot{q}_1\dot{q}_4 + \tfrac{1}{2}(\beta_{125} + \beta_{251} - \beta_{152})\dot{q}_1\dot{q}_5 + \beta_{223}\dot{q}_2\dot{q}_3 + \beta_{224}\dot{q}_2\dot{q}_4 + \beta_{225}\dot{q}_2\dot{q}_5 + \sigma_{223}q_2q_3 + \sigma_{224}q_2q_4 + \sigma_{125}q_1q_5 + \sigma_{1122}q_1^2q_2 + \sigma_{1111}q_2^3 = 0 \tag{22d}$$

$$\mu_{33}\left(\ddot{q}_3 + 2\zeta\nu_3\dot{q}_3 + \nu_3^2 q_3\right) + \tfrac{1}{2}(\beta_{131}q_1 + \beta_{132}q_2)\ddot{q}_1 + \tfrac{1}{2}(\beta_{231}q_1 + \beta_{232}q_2)\ddot{q}_2 + \tfrac{1}{2}(\beta_{131} - \beta_{113})\dot{q}_1^2 + \tfrac{1}{2}(\beta_{232} - \beta_{223})\dot{q}_2^2 + \tfrac{1}{2}(\beta_{132} + \beta_{231} - \beta_{123})\dot{q}_1\dot{q}_2 + \tfrac{1}{2}\sigma_{113}q_1^2 + \tfrac{1}{2}\sigma_{223}q_2^2 = C_q \tag{22e}$$

$$\mu_{44}\left(\ddot{q}_4 + 2\zeta\nu_4\dot{q}_4 + \nu_4^2 q_4\right) + \tfrac{1}{2}(\beta_{141}q_1 + \beta_{142}q_2)\ddot{q}_1 + \tfrac{1}{2}(\beta_{241}q_1 + \beta_{242}q_2)\ddot{q}_2 + \tfrac{1}{2}(\beta_{141} - \beta_{114})\dot{q}_1^2 + \tfrac{1}{2}(\beta_{142} + \beta_{241} - \beta_{124})\dot{q}_1\dot{q}_2 + \tfrac{1}{2}(\beta_{242} - \beta_{224})\dot{q}_2^2 + \tfrac{1}{2}\left(\sigma_{114}q_1^2 + \sigma_{224}q_2^2\right) = 0 \tag{22f}$$

$$\mu_{55}\left(\ddot{q}_5 + 2\zeta\nu_5\dot{q}_5 + \nu_5^2 q_5\right) + \tfrac{1}{2}(\beta_{151}q_1 + \beta_{152}q_2)\ddot{q}_1 + \tfrac{1}{2}(\beta_{251}q_1 + \beta_{252}q_2)\ddot{q}_2 + \tfrac{1}{2}(\beta_{151} - \beta_{115})\dot{q}_1^2 + \tfrac{1}{2}(\beta_{152} + \beta_{251} - \beta_{125})\dot{q}_1\dot{q}_2 + \tfrac{1}{2}(\beta_{252} - \beta_{225})\dot{q}_2^2 + \sigma_{125}q_1q_2 = 0 \tag{22g}$$

The coefficients in the preceding equations are all dimensionless, among which α_i, β_{ijk}, β_{ijkl}, μ_{ij}, σ_{ijk}, σ_{ijkl}, and C_q are integrals of complicated modal functions. Also, α_1 and α_2 are coupling coefficients between the spring–damper–mass vibration and the primary modal sloshing. The terms with coefficients β_{ijk}, β_{ijkl}, or μ_{ij} represent the inertial forces of the finite-amplitude sloshing. The terms with coefficients σ_{ijk} or σ_{ijkl} result from the surface tension. It is obvious that the surface tension provides complicated nonlinear-spring terms in Eq. (22).

Because of the geometrical symmetry between the degrees of freedom for the X and Y motion and between the sloshing modes, there is symbolic symmetry between the corresponding equations and between the corresponding terms in any single equation. The motions in X and q_1 are coupled even for the linearized system and so are the motions Y and q_2. However, if a small excitation is applied only in the X direction, a weak nonlinearity exists in the response of the coupled chain $X \sim q_1$ due to the participation of the high-order planar modes. The chain $Y \sim q_2$ is similar.

By this token, $X \sim q_1 \sim q_3 \sim q_4$ and $Y \sim q_2 \sim q_3 \sim q_5$ form two nonlinearly coupled chains. Increasing the excitation or exciting the system in both the directions will twist the two chains with each other due to the nonlinear coupling of the sloshing modes. In the middle of the two chains, the product terms of q_1, q_2, $\dot{q}_1$, $\dot{q}_2$, $\ddot{q}_1$, and $\ddot{q}_2$ in Eq. (22e) exist in pairs with the same form. At the end of the chains, some corresponding relationships exist in the equations for q_4 and q_5. It is found that there are only the terms with the order of magnitude ε^1 in the equations of X and Y and only ε^2 terms in q_3, q_4, and q_5 equations, but there are ε^1, ε^2, and ε^3 terms in q_1 and q_2 equations, and the ε^2 terms are all coupling ones of the primary sloshing modes.

It follows from the preceding discussion that if an increasing excitation is applied only in one direction, the primary mode must couple with the secondary modes in the same chains first and then with the another primary mode. Thus, all of the terms of order ε^2 must be zeros.

The conclusion is supported by numerical simulations that show that, in Eq. (22), the magnitudes of β_{111}, β_{112}, β_{115}, β_{121}, β_{122}, β_{123}, β_{124}, β_{132}, β_{142}, β_{151}, β_{221}, β_{231}, β_{241}, β_{222}, β_{225}, β_{252}, β_{1112}, β_{1211}, β_{1222}, and β_{2212} are less than the magnitudes of the other coefficients by a factor of 10 or more.

Numerical Method

For simplicity, we constrain the motion to be only in the X direction, that is, $Y = 0$. The coupled equations can be rewritten as

$$[\tilde{M}]\{\ddot{\tilde{P}}\} = \{\tilde{F}\} \tag{23}$$

where $[\tilde{M}]_{6\times 6}$ is a function of the generalized coordinates,

$$\{\ddot{\tilde{P}}\} = \{\ddot{X}, \ddot{q}_1, \ddot{q}_2, \ddot{q}_3, \ddot{q}_4, \ddot{q}_5\}^T \tag{24}$$

is the nondimensional acceleration vector, and $\{\tilde{F}\}_{6\times 1}$ is a function of the generalized coordinates, their time derivatives, and the nondimensional time. It is obvious that the matrix $[\tilde{M}]$ must be positive definite. Equation (23) can be rewritten as

$$\{\ddot{\tilde{P}}\} = [\tilde{M}]^{-1}\{\tilde{F}\} \tag{25}$$

From Eq. (25), a state-space form of the mathematical model is easily obtained and solved by the classical Runge–Kutta method.[12] The discretization error and the roundoff error of the method can be found in Ref. 12. Many numerical experiments have been done. It is found that the algorithm is convergent with an abundant choice of step sizes. The simulated system and the initial values are given in the following sections. There are many parameters included in this mathematical model, such as the scale of the tank, the Bond number, the mass and the frequency ratios of the coupled system, etc. Numerical simulations show that the damping coefficients of the coupled system and the amplitude and frequency of excitation have remarkable effects on the convergence of the numerical results.

To gain an insight into a nonlinear system, it is not enough to give numerical solutions for some initial values. It is known that the frequency-response curves of some state variables can be obtained by experiments in which the excitation frequency increases slowly and uniformly with time. By analyzing the experimental results carefully, we know that the nonlinear vibration system would take the steady state (displacements, velocities, and the amplitude and phase of the excitation) of the last sample as its initial conditions when the frequency is changed to a new sample. This is the primary cause of a hysteretic jump phenomenon of the amplitude-frequency curves that takes place in the experiments. It is easy to realize that any algorithms can produce the same curves if they simulate the process of the experiment. We call these algorithms experiment-simulating algorithms.

Synchronous Hopf-Bifurcation Phenomenon of the Nonplanar Sloshing Modes in the Coupled System

A coupled system without a baffle, with the following parameters and analogous to the experimental system in Ref. 4 is called system A and is investigated first: $d = 3.1$, $h = 3.0$, $g = 1.0$, $B_0 = 66$, $\Gamma = 0$, $\mu = 0.1600$, $\nu_1 = 0.9000$, $\theta_c \approx 0$, $\zeta_1 = \zeta_2 = 0.0348$, $\zeta_3 = \zeta_4 = \zeta_5 = 0.035$, and $\zeta_x = 0.05$.

For example 1, the nondimensional amplitude of the excitation is 0.01, the nondimensional frequency 0.80, and the step size 0.1. Small initial values $q_2 = 0.01$ and $q_5 = 0.001$ for the nonplanar sloshing modes and zero for the other state variables are assumed. The histories of the generalized coordinates are given in Figs. 2a–2f and that of the wave height at point $(r, \theta) = (a, 0)$ is given in Fig. 2g.

In example 2, the frequency is changed to 0.90. The time histories are given in Fig. 3.

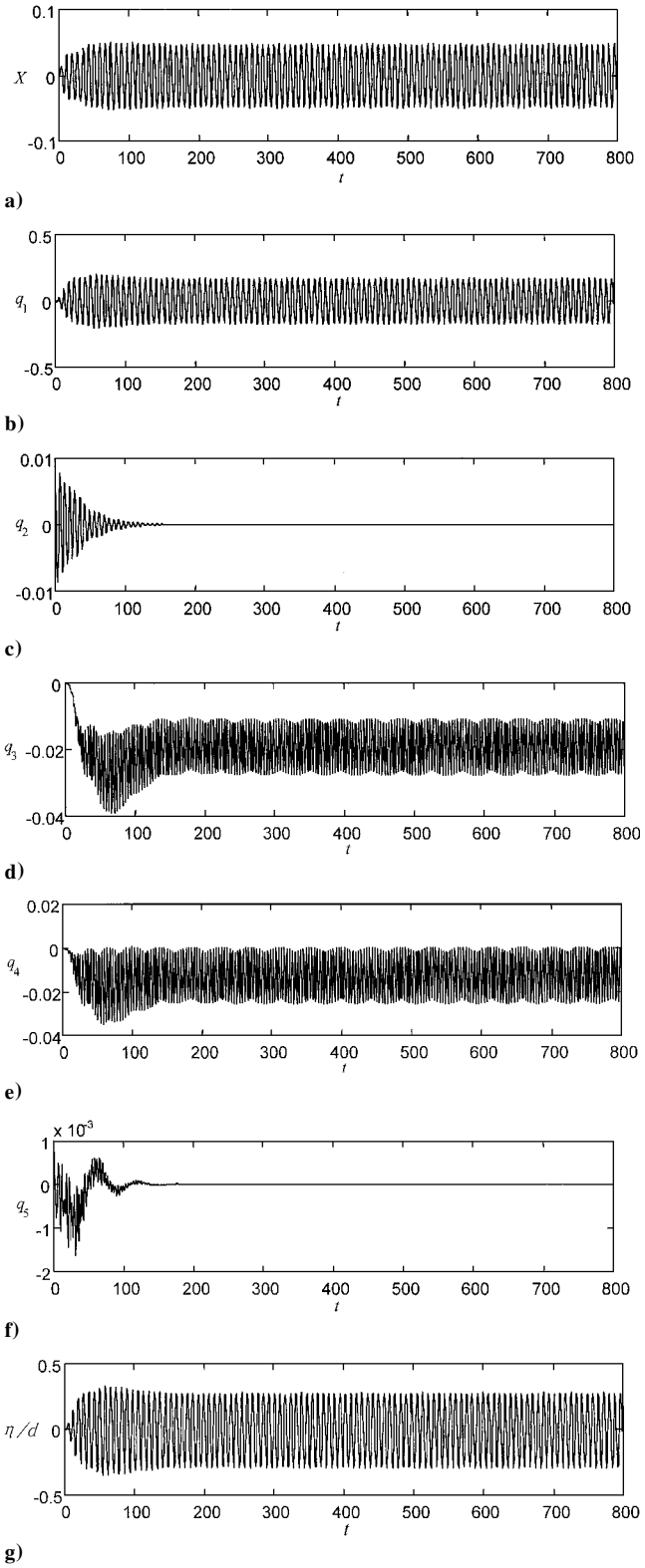

Fig. 2 Time histories of system A; $E_{ex} = 0.010$ and $\nu_x = 0.80$.

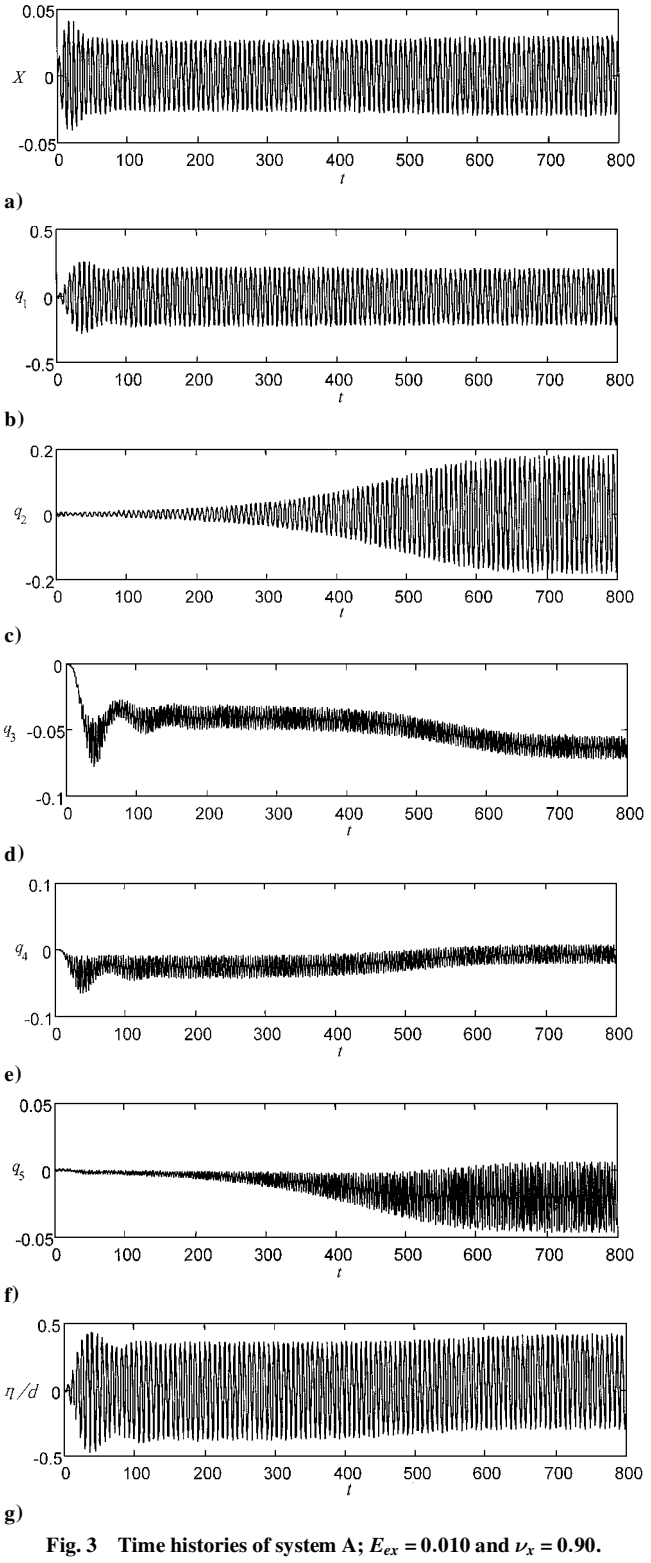

Fig. 3 Time histories of system A; $E_{ex} = 0.010$ and $\nu_x = 0.90$.

By comparing the examples, we found that a small change in the excitation frequency has led to a significant change in the dynamic behavior of the coupled system: 1) the primary nonplanar sloshing mode going from converging on zero to unstable, 2) the secondary nonplanar mode becoming unstable, 3) the amplitude of the response in q_1 increasing remarkably, and 4) the zero-drift phenomenon of the wave height taking place. Many runs with different initial conditions have been done, showing that the listed phenomena are repeatable.

Large initial conditions in the examples are adapted for a glaring representation of the phenomenon. In fact, even a small perturbation or just a perturbation in one of the nonplanar sloshing modes can produce the phenomena as well, but the transition time is longer.

For example 3, all of the initial conditions are zero and the results are given in Fig. 4. From Fig. 4, it is shown that the numerical solution for the unstable equilibrium (no nonplanar sloshing) of system A does exist for sure when $E_{ex} = 0.010$ and $\nu_x = 0.90$.

In fact, the Hopf bifurcation of the primary nonplanar sloshing mode takes place when the excitation frequency changes from 0.80 to 0.90. In the phase plane $(q_2, \dot{q}_2)$, the attractor changes into a stable limit cycle from a focus at the origin, as Fig. 5 shows.

Note that while bifurcation of the primary nonplanar mode takes place, the bifurcation of the secondary nonplanar mode also does, as shown in Fig. 6 and by comparing Figs. 2 and 3.

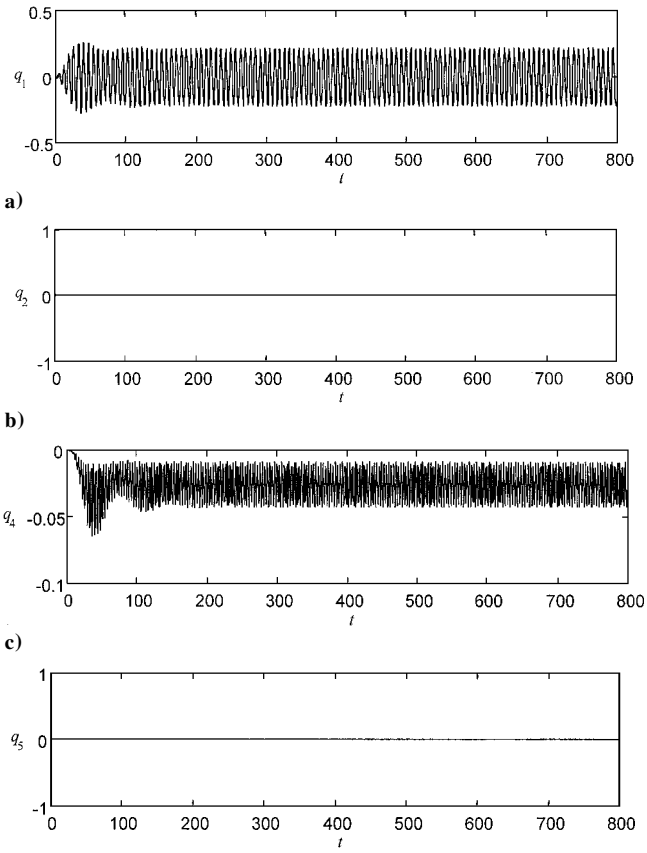

Fig. 4 Time histories of system A; $E_{ex} = 0.010$, $\nu_x = 0.90$, and zero initial conditions.

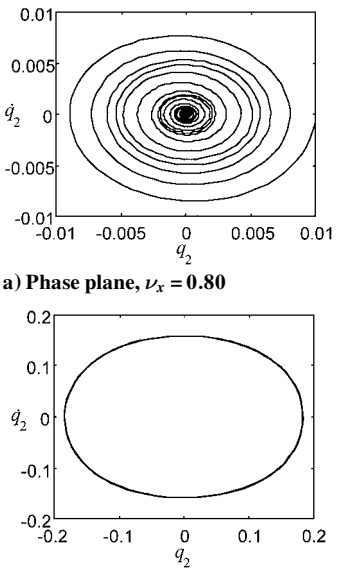

Fig. 5 Supercritical bifurcation of nonplanar primary mode, system A; $E_{ex} = 0.010$.

Numerical simulations show that the bifurcation parameters (frequencies) of the primary and secondary nonplanar modes are identical for the same excitation amplitudes. With regard to system A for $E_{ex} = 0.010$, the bifurcation frequency is $\nu_x = 0.8875$. Similarly, the excitation amplitudes corresponding to the Hopf-bifurcation points for the two degrees of freedom are identical for the same excitation frequencies. The phenomenon of Hopf-bifurcation taking place in two or more degrees of freedom at the same point of the parameter space is called synchronous Hopf bifurcation in this paper. In fact, here both the harmonic-excitation amplitude and frequency can be the parameters of the Hopf bifurcation. Through numerous numerical simulations, a bifurcation set can be determined in the parameter space for the nonplanar modes of system A.

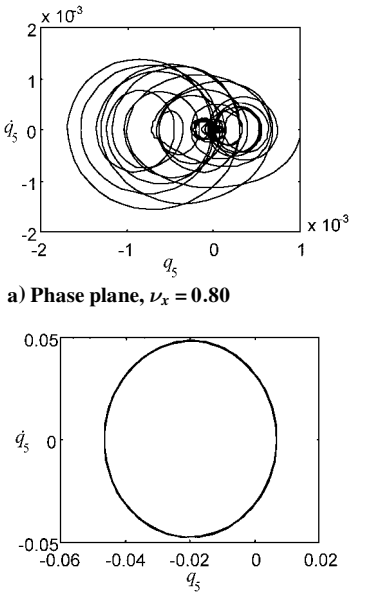

Fig. 6 Supercritical bifurcation of nonplanar secondary mode, system A; $E_{ex} = 0.010$.

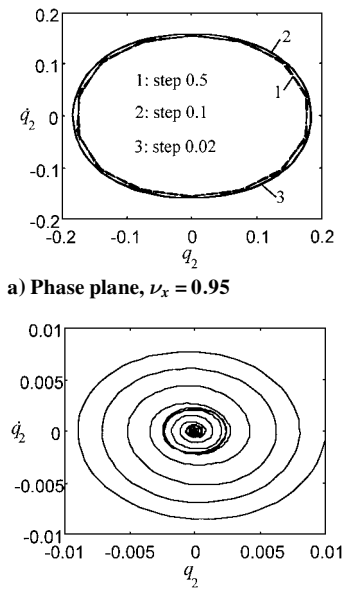

Fig. 7 Subcritical bifurcation of the nonplanar primary mode, system A; $E_{ex} = 0.010$.

The preceding synchronous Hopf bifurcation is the first one of system A. It occurs at the right-hand side of the bifurcation parameters and is a supercritical bifurcation. Synchronous bifurcation of the nonplanar modes of system A takes place for the second time when $\nu_x = 0.9505$ and $E_{ex} = 0.010$. The phase diagrams of the primary and secondary modes with $\nu_x = 1.0$ and $E_{ex} = 0.010$ are given in Figs. 7b and 8b. The second synchronous bifurcation is a subcritical one. The steady results with different integral steps used are plotted in Figs. 7a and 8a, and they show the accuracy and grid independence of the numerical simulations.

Reviewing the described process, by using the polar coordinates to describe the modal attractors of the two nonplanar modes, we specify the average polar radius of the primary mode as r_2 and specify that of the secondary modes as r_5. With a fixed excitation amplitude, the locus of the nonplanar modes sloshing is shown in Fig. 9 in the product space (r_5, r_2, ν_x) of the generalized phase space and the parameter space.

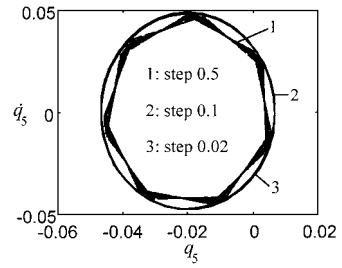

a) Phase plane, $\nu_x = 0.95$

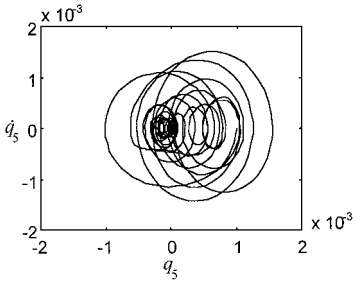

b) Phase plane, $\nu_x = 1.0$

Fig. 8 Subcritical bifurcation of nonplanar secondary mode, system A; $E_{ex} = 0.010$.

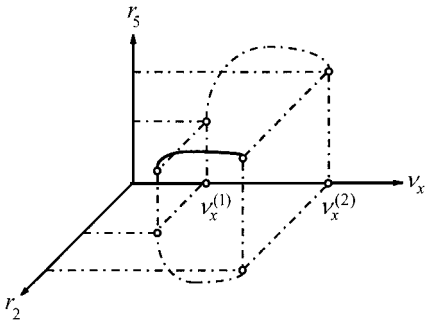

Fig. 9 Synchronous Hopf bifurcation.

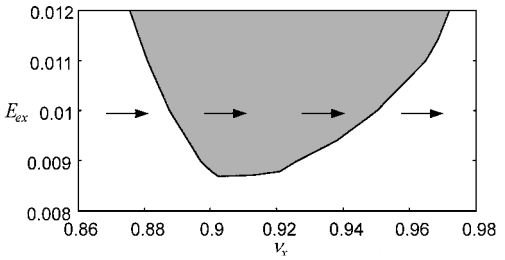

Fig. 10 Synchronous Hopf-bifurcation set of nonplanar modes of system A.

In Fig. 9, the solid curve, known as a bifurcation track, represents a series of motion states of system A. The dashed curve in the plane (r_2, ν_x) is a projection of the bifurcation track in the plane $r_5 = 0$. In fact, it is the bifurcation diagram of the primary mode. The other dashed curve is the projection of the track in the plane $r_2 = 0$, which is the bifurcation diagram of the secondary mode. For $E_{ex} = 0.010$, the nondimensional frequencies of the two Hopf bifurcations are $\nu_x = 0.8875$ and 0.9505. Figure 10 shows the bifurcation set in parameter plane (ν_x, E_{ex}). The shadowed area presents the existence of stable nonplanar sloshing.

As a supplement, the preprocessing gives the first-order nondimensional sloshing frequency $\nu_1 = 0.9024$ and also two coupled system frequencies $\nu_a = 0.8428$ and $\nu_b = 1.0101$ without damping. Figure 10 shows that the frequency exciting the nonplanar sloshing of the coupled system is about the same as the first-order sloshing frequency and is between the two coupled system frequencies. In this section, the synchronous Hopf-bifurcation phenomenon is given by several special numerical examples. As a matter of fact, numerical simulations show that the phenomenon is a general behavior of the coupled system. In Fig. 10, it is shown that while $E_{ex} \geq 0.0087$, the bifurcation may appear. While $E_{ex} \leq 0.015$, the numerical results of system A always give the described phenomenon. While the damping ratios decrease to two-thirds of the system with $E_{ex} = 0.010$, the results will diverge as well.

As shown in Figs. 2b, 2g, and 3, the response for the other degrees freedom changes significantly when the bifurcation of the nonplanar modes takes place. For instance, as a comprehensive result, the time history of the wave height at a special point has a significant zero-drift after bifurcation.

In Eq. (22), the equation corresponding to each secondary mode contains many square terms of the primary modal coordinates, which are the source of the zero-drift phenomenon. When the supercritical synchronous Hopf bifurcation of the nonplanar modes takes place, the zero-drift driven by the primary modes becomes more significant. According to this analysis, the synchronous Hopf-bifurcation point of the nonplanar modes is also the catastrophic point of system A at which the response of each state variable changes greatly.

It follows from the discussion of dynamic modeling that in the sense of linearity the vibration of X is coupled with the planar asymmetrical primary sloshing modal. When the amplitude of the sloshing is large enough, the planar primary modal motion will drive the planar secondary mode and the axial symmetrical mode due to the strong coupling of the chain $q_1 \sim q_3 \sim q_4$. When the amplitude of the excitation increases to a large enough value, the nonplanar sloshing will become unstable and obtain kinetic energy from the planar modes. Then, because of the strong coupling of the nonplanar modes, synchronous Hopf bifurcation takes place. In conclusion, the synchronous bifurcation phenomenon is an important representation of the sophisticated behavior of the nonlinear system A.

Damping Osmosis Phenomenon of the Coupled System

In space engineering, liquid sloshing usually needs to be suppressed. The best way to improve the sloshing damping is usually to install baffles in the tank. At present, it is clear how the rigid baffles affect the dynamic characteristics of the sloshing liquid. A liquid–spacecraft coupled system B is investigated in this section. The parameters of system B are as follows: $d = 29.2$, $h = 18.05$, $g = 1.0$, $B_0 = 2870$, $\Gamma = 0$, $\mu = 0.8253$, $\nu_1 = 0.8495$, $\theta_c \approx 0$, $\zeta_1 = \zeta_2 = 0.0019$, $\zeta_3 = \zeta_4 = \zeta_5 = 0.0012$, $\zeta_{xs} = 0.098$, and $\zeta_{xb} = 0.15$.

The two linear coupled system frequencies are $\nu_a = 0.6617$ and $\nu_b = 1.0384$. The zero initial conditions with small pertubations in the nonplanar modal coordinates are adopted as well in the following numerical example. As a numerical example, the amplitude of the excitation is 0.010, and the integral step size is 0.5. An annular baffle with width $w = 1.35$ cm and immerged depth $D = 1.50$ cm is installed in the cylindrical tank. With the use of the experiment-simulation algorithm, the amplitude-frequency response curves of system B are plotted in Fig. 11. In the algorithm, the excitation frequency increases with a small step 0.01. At each frequency, long-time histories of the system from $t = 0$ to 2500 have been simulated to obtain steady amplitudes of X: q_1 and q_2.

Comparing the results for the cases without and with a baffle in Fig. 11, we find the functions of the baffle to be 1) always suppressing significantly the amplitude of the liquid sloshing and the nonplanar sloshing bifurcation in the tanks, 2) having a complicated effect on the vibration of the spring–mass system and sometimes suppressing the vibration and sometimes amplifying the vibration, 3) suppressing significantly the zero drifts of each modal coordinate, and so suppressing the whole liquid sloshing, etc.

It is noticed that phenomenon 2 takes place in the case of the harmonic force by which the planar and nonplanar sloshing will be excited significantly when the baffle is removed. When it is presumed that a wide baffle is installed at the liquid free surface and the liquid is sealed as a rigid mass, the coupled system will degenerate into a spring–mass system with a single degree of freedom, and the mentioned phenomenon will be the resonant behavior of the system. The curves in Fig. 11a are analogous to those of the dynamic damper with different dampings in the linearized system. Phenomenon 2 can be viewed as the damping effects of the baffle in the liquid–solid coupled system. When the baffle is removed or when the width

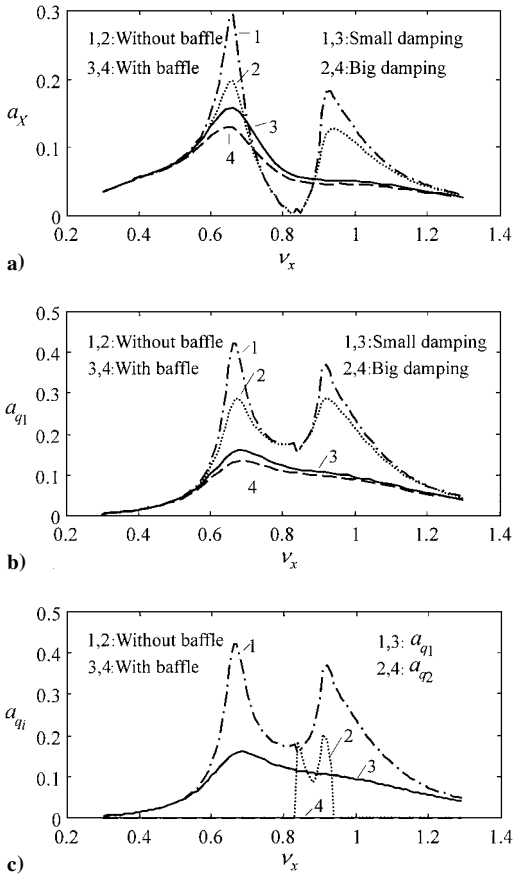

Fig. 11 Effect of damping on the amplitude-frequency characteristic of system B.

of the baffle is small enough, there are at least two characteristic peaks (maybe three or more if the nonplanar sloshing is excited) corresponding to the two linear coupled frequencies. A baffle with a moderate width will amplify the vibration of the spring–mass system at the first-order slosh eigenfrequencies. In fact this is also a result of the baffle suppressing the liquid sloshing significantly. A conclusion can be made that the baffle does not always work better as its width increases. It works best only for a certain width from the viewpoint of liquid–spacecraft coupled dynamics. From Eq. (18), it is easy to see that the sloshing damping is increasing and effect 2 is becoming more significant while the baffle is getting wider and the immerged depth is getting smaller.

Comparing the results for small vs large vibration damping, we notice that 1) the damper suppresses both the vibration and the sloshing and 2) the suppressing effect of the damper on the sloshing is smaller than that of the baffle.

These effects are understandable. With the increase of the damping, the amplitude of the vibration decreases, which means the decrease of the kinematic excitation to the liquid sloshing. Therefore, the amplitude of the liquid sloshing will decrease. As for effect 2, it is mainly because the damping of the damper is usually not too great. The baffle works directly on the liquid, and so the effect is usually significant.

The dual suppressing effects of the damper on the vibration and the sloshing are meaningful for engineering. For instance, one can intentionally design joints with adequate damping to passively suppress the vibration of the whole spacecraft.

To summarize, in the liquid–spacecraft coupled system, the damper damping always permeates through the liquid to suppress both the sloshing and the elastic vibration. The baffle suppresses the liquid sloshing remarkably, but affects the elastic vibration in different ways according to the different excitation frequencies. If the excitation frequency is far away from the first-order sloshing, the baffle damping will permeate through the spring–mass system. If the excitation is near the sloshing frequency, it will become a negative damping, which amplifies the elastic vibration. Therefore, the described phenomenon can be called damping osmosis of the liquid–spacecraft coupled system, which is a nonlinear phenomenon.

Conclusions

The mathematical model of a simplified nonlinear liquid–spacecraft coupled dynamic system is established by symbolic operation of the software *Mathematica*. Several important dynamic phenomena of the system are found by numerical simulations.

Because of the geometrical symmetry of the physical model, the mathematical model presents symmetry between equations and between terms within a single equation, which proves that the dynamic equations are correct to some extent.

Numerical simulations of the system without a baffle indicate that a synchronous Hopf bifurcation may occur for the nonplanar sloshing modes of the coupled system subject to only planar excitation with slowly increasing frequency. The supercritical and subcritical bifurcation frequencies are located behind and in front of the first-order eigenfrequency of the liquid sloshing, respectively.

The synchronous Hopf bifurcation is the representation of the sophisticated nonlinear coupled relationships. When the bifurcation takes place, the dynamic behaviors of the whole system change significantly. For instance, the time history of the wave height presents a remarkable zero-drift phenomenon.

Another nonlinear phenomenon, the damping osmosis, appears when an annular baffle is installed in the cylindrical tank in the coupled system. For a forced system, the damping of the elastic vibration always permeates through the liquid to suppress the sloshing while suppressing the vibration. The baffle suppresses the sloshing significantly, but has different effects on the elastic vibration, depending on the excitation frequency.

The concept of synchronous Hopf-bifurcation phenomenon deepens our insights into the nonlinear coupled liquid–spacecraft system. The damping osmosis phenomenon demonstrates that although the baffle is an efficient means of passively controlling the liquid–spacecraft coupled system, it is not necessarily the wider the better, and its size should be optimized.

References

[1]Cendral, J. L., and Berry, W., "ESA's Activities in the Fields of Dynamics and Technology Related to the Presence of Liquids On-Board Spacecraft," *Proceedings of the CNES–ESA Conference on Attitude Control of Space Vehicles—Technological and Dynamic Problems Associated with the Presence of Liquids*, Oct. 1977, pp. 9–21.

[2]Buseck, R., and Benaroya, H., "Mechanical Models for Sloshing of Liquid Fuel," AIAA Paper 93-1093, Feb. 1993.

[3]Chu, W. H., "Low-Gravity Fuel Sloshing in an Arbitrary Axisymmetric Rigid Tank," *Transactions of the American Society of Mechanical Engineers*, Vol. 92, No. 3, 1970, pp. 828–837.

[4]Peterson, L. D., Crawley, E. F., and Hansman, R. J., "The Nonlinear Dynamics of a Spacecraft Coupled to the Vibration of a Contained Fluid," AIAA Paper 88-2470, April 1988.

[5]van Schoor, M. C., and Crawley, E. F., "Nonlinear Forced-Response Characteristics of Contained Fluids in Microgravity," *Journal of Spacecraft and Rockets*, Vol. 32, No. 3, 1995, pp. 521–532.

[6]Miles, J. W., "Nonlinear Surface Waves in Closed Basins," *Journal of Fluid Mechanics*, Vol. 75, 1976, pp. 419–448.

[7]Hutton, R. E., "An Investigation of Resonant, Nonlinear, Nonplanar Free Surface Oscillations of a Fluid," NASA TN D-1870, 1963.

[8]Nagata, M., "Nonlinear Faraday Resonance in a Box with a Square Base," *Journal of Fluid Mechanics*, Vol. 209, 1989, pp. 265–284.

[9]Komatsu, K., "Nonlinear Sloshing Analysis of Liquid in Tanks with Arbitrary Geometries," *International Journal of Nonlinear Mechanics*, Vol. 22, No. 3, 1987, pp. 193–207.

[10]Miles, J. W., "Resonantly Forced Surface Waves in a Circular Cylinder," *Journal of Fluid Mechanics*, Vol. 149, 1984, pp. 15–31.

[11]Miles, J. W., "Ring Damping of Free Surface Oscillation in a Circular Tank," *Journal of Applied Mechanics*, Vol. 25, No. 2, 1958, pp. 274–276.

[12]Henrici, P., *Discrete Variable Methods in Ordinary Differential Equations*, Wiley, New York, 1962, pp. 108–157.

P. Givi
Associate Editor